Arabian Journal of Geosciences (2020) 13: 809
https://doi.org/10.1007/s12517-020-05820-x

ORIGINAL PAPER

Petrology and geochemistry of the Lattan Mountain magmatic rocks in the Sanandaj–Sirjan Zone, west of Iran

Maryam Ahankoub[1] · Yoshihiro Asahara[2] · Motohiro Tsuboi[3]

Received: 28 May 2020 / Accepted: 30 July 2020 / Published online: 17 August 2020

Abstract

Igneous rocks are distributed in the Lattan Mountain area, the center part of Sanandaj–Sirjan Zone, west Iran. Based on the mineralogy and geochemical composition, these are subvolcanic, volcanic, and plutonic rocks. It includes basalts, andesitic basalt, and andesite, with porphyritic to microlithic porphyry and vitrophyric textures as well as dolerite, diorite, gabbro, and microdiorite with a varied granular, microgranular, intersertal, and intergranular textures. The chemical compositions indicated to calc-alkaline to transitional nature, enrichment in LIL elements (Rb, Ba, Th, U, and Pb), and depletion in Ti and Zr, as it is evident in spider diagrams normalized to a primitive mantle. In addition, samples have enrichments of LREE relative to HREE. The Rb-Sr whole-rock isochron of these magmatic rocks shows an age of 152 ± 14 Ma (late Jurassic). The initial $^{87}Sr/^{86}Sr$ (0.7047 to 0.7051) and $^{143}Nd/^{144}Nd$ ratios range from (0.512534 to 0.512710) and εNdt = − 0.1 to + 2.2 that indicated to BSE composition. Our results suggest that the magmas for the magmatic rocks were derived from metasomatized enriched MORB-like sources. These rocks were formed in an island arc setting during subduction and closure of the Neotethys oceanic lithosphere beneath the Iran microplate about 152 Ma.

Keywords Island arc magmatism · Calc-alkaline to transitional nature · Subduction · Lattan Mountain · Sanandaj · Sirjan Zone

Introduction

The Neotethys orogenic belt was developed as a result of geodynamic processes in the Mesozoic and Cenozoic eras and includes several phases of subduction, abduction, microplate accretion, continent–continent collision, and exhumation (Dercourt et al. 1986; Hafkenschied et al. 2006). The Jurassic northeastward subduction of the Neotethys occurred beneath the eastern European (i.e., Eurasian margin caused continuous active arc magmatism along the eastern Pontides, the Lesser Caucasus, and the Sanandaj–Sirjan Zone (SaSZ)) (Kazmin et al. 1986; Ustaömer and Robertson 1999; Davoudian et al. 2016). The SaSZ is a narrow belt of highly deformed and metamorphosed rocks in the Zagros orogeny with NW–SE structure trend, associated with abundant deformed and undeformed plutons, as well as widespread Mesozoic volcanics (Eftekharnejad 1981; Berberian and Berberian 1981; Mohajjel and Fergusson 2000; Babaie et al. 2001; Mohajjel et al. 2003; Azizi and Jahangiri 2008; Shahbazi et al. 2010; Azizi et al. 2011; Mahmoudi et al. 2011; Esna-Ashari et al. 2012; Azizi et al. 2014; Azizi et al. 2015a, b; Azizi et al. 2016; Davoudian et al. 2016; Hassanzadeh and Wernicke 2016; Azizi et al. 2018a, b). The volcanic rocks of the marginal subzone are interpreted to represent volcanic rocks that accumulated in a forearc basin located along the southwestern margin of the Urumieh-Dokhtar magmatic arc (Alavi 1994).

Responsible Editor: Federico Lucci

✉ Maryam Ahankoub
Ahankoub_m@yahoo.com

Yoshihiro Asahara
asahara@eps.nagoya-u.ac.jp

Motohiro Tsuboi
tsuboimot@kwansei.ac.jp

1 Department of Geology, Faculty of Science, University of Payame, Noor, Iran

2 Department of Earth and Environmental Sciences, Graduate School of Environmental Studies, Nagoya University, Nagoya 464-8601, Japan

3 Department of Applied Chemistry for Environment, School of Science and Technology, Kwansei Gakuin University, Sanda 669-1337, Japan

These volcanic rocks are interbedded with detrital sediments such as black shale, sandstone, and sandy limestone (Zahedi et al. 1992). Kazmin et al. (1986) believed that the Mesozoic volcanic rocks of the SaSZ were formed in Jurassic. $^{49}Ar/^{48}Ar$ dating of the volcanic rocks of Shahrekord indicates 145 to 169 Ma age with calc-alkaline and toleiitic nature that was formed in island arc setting (Emami et al. 2009). Zarasvandi et al. (2015) believed that during ocean–ocean subduction in Jurassic to Cretaceous, an immature island arc developed before the closure of Neo-Tethys Ocean in SSZ, while an intercontinental rifting regime is considered to be the formation environment of the Jurassic rocks in the northern of the SaSZ (Azizi et al. 2018a, b). Also, chemical composition of Panjeh mafic and intermediate rocks, in combination with data for other gabbroic to dioritic bodies in the Ghorveh area, offers two interpretations for these (and other Jurassic igneous rocks of the SaSZ) as reflecting melts from (a) subduction-modified OIB-type source above a Neo-Tethys subduction zone or (b) plume or rift tectonics involving upwelling metasomatized mantle (Azizi et al. 2018a, b). The narrow belt of black and green–colored magmatic rocks in the Lattan Mountain extends NW–SE in the north of Chaharmahal and Bakhtiyari provinces that is parallel to the main Zagros fault and 35 km distanced from it (Fig. 1). There are no other detailed geochemical and isotopic studies on the Lattan Mountain magmatic rocks (e.g., their nature, source, and age). In this paper, petrography, whole-rock geochemistry, and Sr-Nd isotopic ratios are used to constrain Lattan Mountain magma genesis and its tectonic setting.

Geological setting

The Lattan Mountain (LM) is located between the longitude 50° 42′ E to 51° 10′ E and the latitude 32° 45′ N to 32° 08′ N (Fig. 2). It lies within the highly deformed subzone of the SaSZ (Zahedi et al. 1992). The typical lithology of the study area is similar to those of the other parts of the SaSZ which are exposed around the east of Zagros Thrust Fault. In general, the stratigraphical units of the LM can be divided into two main parts that are affected by the Neotethys events: before and after the Permian (Zahedi et al. 1992). The Permian units consist of light to gray thick-bedded and extremely folded dolomite with a thickness of over several tens of centimeters and with inverse fault (Zahedi et al. 1992). Permian layers have a discontinuous erosional boundary with Triassic detrital and carbonate units, and there are some traces of Cu mineralization. The Jurassic units include volcanic rocks with dark gray limestone layers and slight sandstone, and shale that was extended from north to south of Shahrekord. This limestone is folded and displays abundant cracks and fractures, which is covered with Cretaceous limestone and sandy limestone and argillitic limestone. The alternate Miocene-Pliocene units, with various thicknesses from 1 to 2 m, include gray-green marls, gray sandstones, and light gypsum that are located

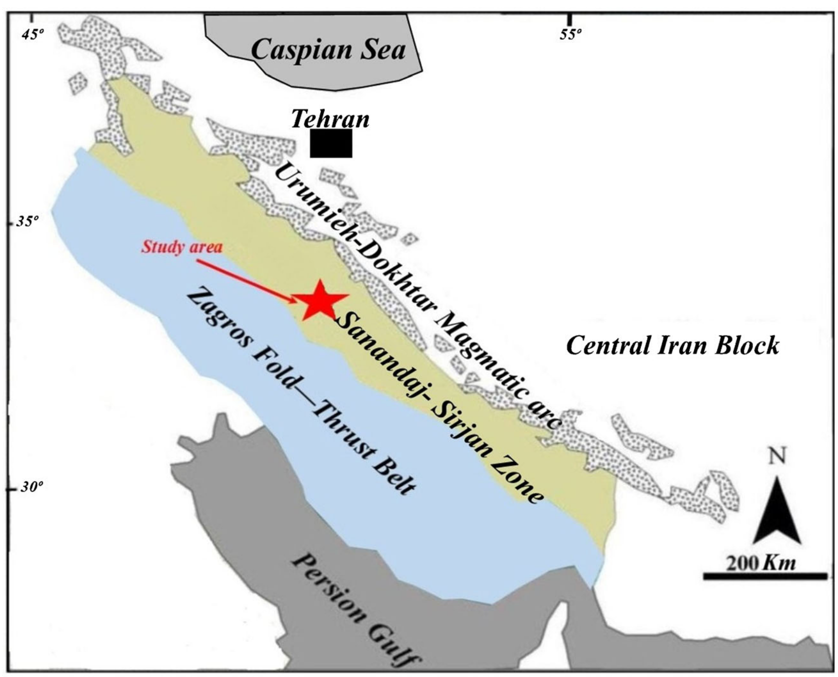

Fig. 1 Geological map of the Zagros orogenic belt (modified from Alavi (2004))

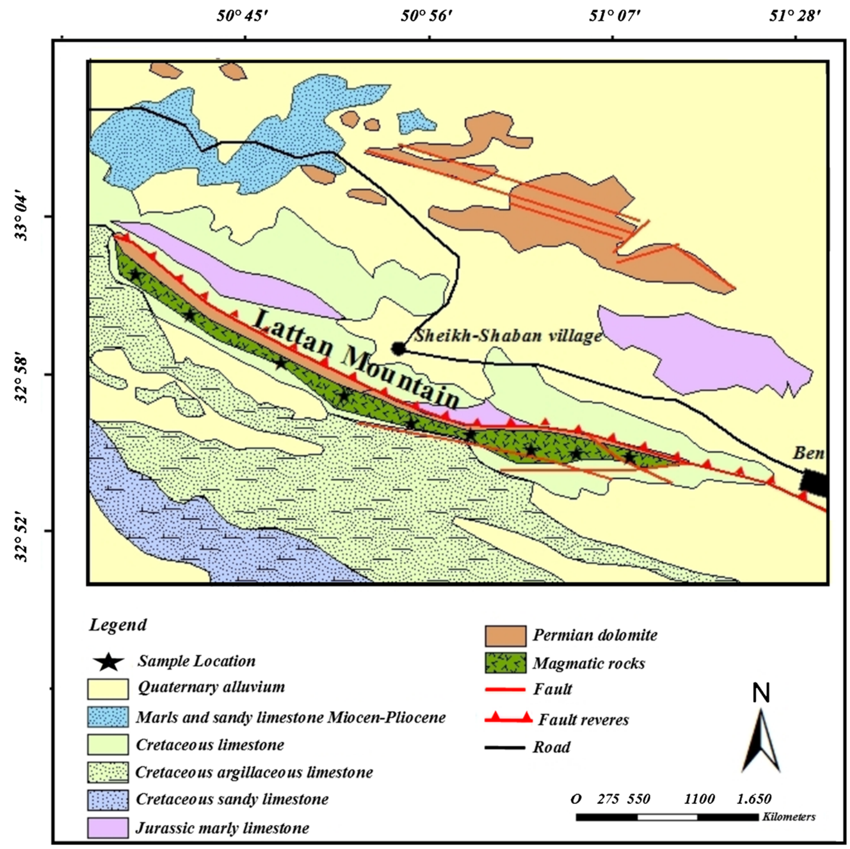

Fig. 2 The geological map of the LM area (Zahedi et al. 1992)

with angular unconformity over older units and are below Quaternary sediments. There are ebony scotella fossils in the limestone layers (Ghasemi et al. 2005). The Quaternary sediments consist of alluvial of clay and silt. In addition, due to Cimmerian orogeny deformation, there are Mesozoic phyllites, schist, and recrystallized limestone. There are metamorphic complexes (metabasite) in the north of the LM that occurred in a-subduction zone setting during late Neoproterozoic to early Cambrian times (Malek-Mahmoudi et al. 2017), while metagranites of the north of LM were mainly produced through mixing of basaltic melts with components similar to metasedimentary source that occurred in Early Paleozoic times after the closure of the Proto-Tethys Ocean (Badr et al. 2018). In the LM, the magmatic rocks are often observed among sedimentary and metamorphic rocks (Fig. 3a). Based on the presence of fossils in the sedimentary rocks, they have been formed in a marine setting in the Jurassic times (Ghasemi et al. 2005). The igneous rocks are found as small to large singular outcrops in the Lattan Mountain area. These magmatic rocks are black to dark gray, green, and gray in color that intrude into the Jurassic to Cretaceous unites (Fig. 3b, c). The volcanic rocks are intermediate to basic terms. The subvolcanic and plutonic rocks are composed of microgabbro, microdiorite, and dolerite as sills and dikes with chilled margins.

In some parts of the LM, malachite, azurite, and hematite, and magnetite mineralization are revealed on the magmatic rocks.

Analytical methods

In this paper, whole-rock analysis for major and trace elements and $^{87}Sr/^{86}Sr$ and $^{143}Nd/^{144}Nd$ isotope ratios was performed for 9 samples. The rock samples were crushed to sizes smaller than 74 μm. Ten major and 14 trace elements were analyzed for nine samples by XRF (Shimadzu XRF-1800) at Kwansei Gakuin University. Loss of ignition (LOI) was calculated by weight difference after ignition at 950 °C. The rock powder samples and flux ($Li_2B_4O_7$) were mixed in proportions of 0.7:6.0 g for major elements and 2.0:3.0 g for trace elements, and the glass beads were prepared for the XRF analysis. As for quantitative analysis of REEs and Sr-Nd isotope analysis, eight of nine samples were prepared through hydrofluoric acid treatment at Nagoya University, Japan. About 100-mg powdered sample was decomposed in HF^+ $HClO_4$ in a covered PTFE beaker. After drying, the samples were re-dissolved in 10 ml of 2–4 M HCl, and the resulting solution was split into two aliquots:

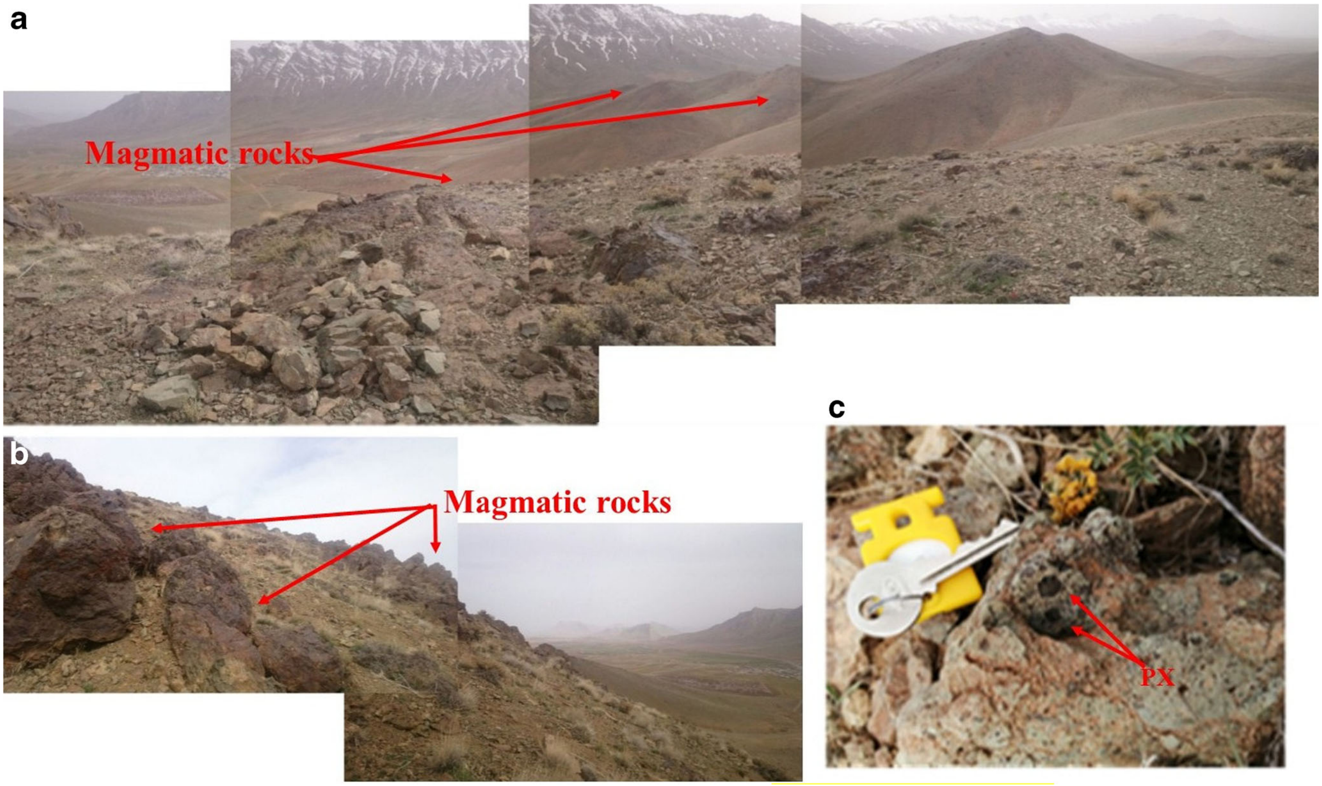

Fig. 3 **a**, **b** Outcrop of the magmatic rocks in Lattan Mountain. **c** Pyroxene in volcanic rocks

one is for REE quantitative analysis and the other for the isotope analysis. The REE concentrations were measured by an Agilent 7700x ICP-MS spectrometer at Nagoya University. For Sr and Nd isotope analysis, conventional column chemistry was conducted to isolate Sr and REEs using cation-exchange resin (Bio-Rad AG50W-X8, 200–400 mesh) with an HCl eluent. Neodymium was separated from the extracted REE fraction by another cation-exchange column with α-hydroxyisobutyric acid (α-HIBA) as eluent. The isotope ratios for the eight samples were obtained using thermal ionization mass spectrometers (TIMS), VG Sector 54-30 for Sr and GVI IsoProbe-T for Nd, at Nagoya University. The mass fractionations during the Sr and Nd isotope measurements were corrected based on $^{86}Sr/^{88}Sr$ = 0.1194 and $^{146}Nd/^{144}Nd$ = 0.7219, respectively. For the samples analyzed at Nagoya University, NIST-SRM987 and JNdi-1 (Tanaka et al. 2000) were adopted as the natural Sr and Nd isotope ratio standards, respectively. The average and 2σ for isotope ratios standards are NIST-SRM987 = 0.710251 ± 0.000020 (n = 8) and JNdi-1 = 0.512114 ± 0.000002 (n = 6).The Sr and Nd isotopic ratio diagram is illustrated using the GCDkit software (Janoušek et al. 2016).

Petrography

Intermediate to basic volcanic, subvolcanic, and plutonic rocks found in Lattan Mountain include andesite, andesitic-basalt, basalt, dolerite, microgabbro, and microdiorite. The volcanic rocks are composed of plagioclase, pyroxene, amphibole, and olivine as major minerals and biotite, apatite, and opaque as accessory ones. The main texture of the volcanic rocks is porphyritic, hypocrystalline porphyritic, hyalo-porphyritic, microgranular, and hyalo-microlithic porphyritic. The microgabbro and microdiorite have small outcrops as sills and dikes with porphyritic to microgranular texture. Their mineralogical constituents of the rocks consist of plagioclase, clinopyroxene, amphibole, and olivine as the major minerals and biotite, apatite, and opaque as accessory minerals. Olivine is mostly observed as anhedral and/or as corroded crystals. The clinopyroxene is mostly observed as microphenocryst and phenocryst. Plagioclase and clinopyroxene minerals are almost fresh, while orthopyroxene minerals are replaced by smectite-chlorite ones (Fig. 4a). The plagioclases are mostly subhedral. The megacryst and phenocryst of the plagioclase exhibit polysynthetic twinning (up to 60%). The basalts consist of plagioclase laths, olivine, and pyroxene glomeroporphyritic aggregations embedded in a glass-poor groundmass that contains small rounded vesicles filled with smectite + epidote + chalcedony. The size of the plagioclase laths ranges from 0.1 to 1 mm (Fig. 4b). The andesites have a number of plagioclase grains with "fritted" rims with a various widths from millimeters to centimeters. Fritted or sieve textures in plagioclase formed in oxidation condition of the subduction setting (Dwijesh et al. 2011). The plagioclase is the

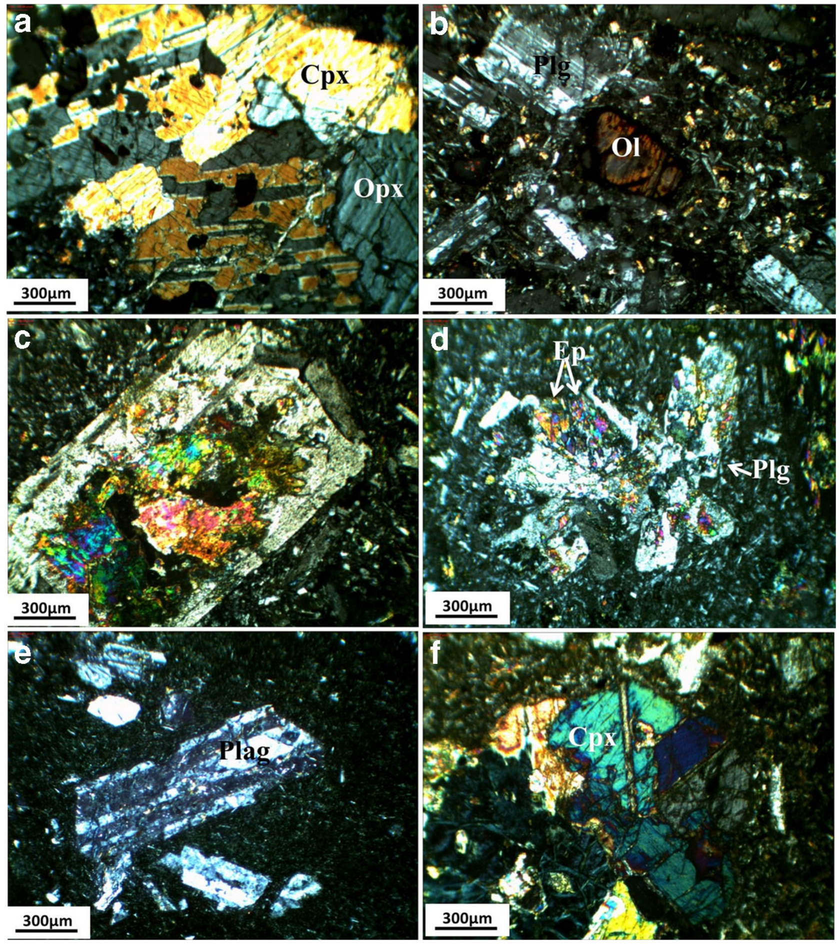

Fig. 4 Photographs of the LM. **a** Pyroxene phenocryst in microgabbro (XPL). **b** Coarse-grained olivine in basalt (XPL). **c** Phenocryst plagioclase and epidote in andesitic basalt (XPL). **d** Secondary epidote in andesite. **e** Plagioclase in andesite (XPL). **f** Cpx in andesite (XPL). Mineral abbreviations are from Whitney and Evans (2010)

main mineral as phenocryst which is mostly replaced by epidote, and clay minerals in the matrix (Fig. 4d–f). Amphibole is common (modal abundances up to 6%). The dolerites, with ophitic to intersertal textures, are composed of plagioclase laths enclosed in anhedral to subhedral clinopyroxene. The clinopyroxene and Fe–Ti oxide occur as large crystals up to 1 and 0.5 cm, respectively (Fig. 4f). The amphibole crystal contains opaque rims. The amphibole is completely pseudomorphed by finely crystalline opaque minerals that indicate oxidation condition and high oxygen fugacity (Popp et al. 2006). There is evidence of the low-grade zeolite and prehnite–pumpellyite facies metamorphism of the igneous rocks while their texture is preserved.

Results

Whole-rock geochemistry

Whole-rock geochemical compositions for the 9 samples of the LM magmatic rocks are presented in Table 1. Most of analyzed rocks show SiO_2 in a range of 46–55 wt%; however, minor dacitic rocks are observed (i.e., sample La5, SiO_2 66.9 wt%). Based on the total of alkalis vs. silica classification diagram of TAS diagram (after Le Bas 2000), the LM rocks plot dominantly in the fields of basalt, basalt andesite, and basaltic trackyandesite and dacite (Fig. 5a). In the AFM diagram (Irvine and Baragar 1971), the Lattan Mountain samples plot in the calc-alkaline domain (Fig. 5b). The Harker diagrams (Harker 1909) show almost negative correlations between SiO_2 and Al_2O_3, Fe_2O_3, TiO_2, CaO, MnO, MgO, Na_2O, and K_2O (Fig. 6). Also, the Lattan Mountain igneous rocks show markedly decreasing values of La, Sr, Eu, Rb, Ba, Zr, Y, and Yb with increasing SiO_2 content (Fig. 7). The chondrite-normalized (Boynton 1984) REE patterns of the samples show LREE enrichment (Fig. 8a). The samples show weak negative Eu anomalies (Eu/Eu* = 0.27–0.33). In the primitive mantle-normalized spider diagram (McDonough and Sun 1995), all of the samples display clear enrichment in Rb, Pb, Sr, and Y and variable depletion in Ba, Th, Zr, and Ti (Fig. 8b). In the diagrams of Th vs. Yb (Barrett and Maclean 1999) and La vs. Yb (Ross and Bédard 2009), the samples were plotted in calc-alkaline to transitional fields (Fig. 9a, b). In Zr/Al_2O_3 vs. TiO_2/Al_2O_3 and La/Yb vs. Th/

Table 1 Whole-rock composition of LM samples

Sample	La1	La2	La3	La4	La5	La6	La7	La8	La9
SiO_2 (wt%)	49.23	51.47	46.94	54.51	66.85	53.75	48.64	50.00	49.52
TiO_2	0.81	0.86	0.86	0.78	0.52	0.77	0.83	0.80	0.88
Al_2O_3	17.55	19.11	18.65	18.16	14.26	18.74	16.24	17.10	19.53
Fe_2O_3	10.25	8.34	10.04	7.74	6.90	7.57	9.43	9.25	9.03
MnO	0.17	0.15	0.15	0.22	0.20	0.18	0.20	0.12	0.15
MgO	7.67	6.58	7.12	6.64	3.48	5.45	9.36	8.58	6.61
CaO	10.11	6.48	8.96	7.37	3.50	8.75	8.59	6.38	7.51
Na_2O	1.73	2.19	2.51	3.10	3.04	2.75	1.43	2.61	2.78
K_2O	0.79	3.64	1.79	1.79	0.36	2.35	1.92	2.21	1.67
P_2O_5	0.21	0.30	0.24	0.30	0.10	0.30	0.27	0.21	0.28
LOI	2.73	2.31	3.98	2.26	1.68	2.04	4.73	4.38	3.47
Total	101.25	101.44	101.24	102.87	100.87	102.66	101.63	101.63	101.42
Ba (ppm)	128	541	260	276	91	277	333	530	279
Rb	24	76	60	37	13	50	78	68	49
Sr	1364	660	603	365	167	442	279	477	413
Zr	47	51	61	47	70	46	64	59	59
Nb	< 1	< 1	< 1	< 1	< 1	< 1	< 1	< 1	< 1
Ni	163	76	200	60	26	54	137	115	147
Co	46	32	57	17	21	19	54	49	40
Zn	68	61	77	50	72	44	75	73	73
Cr	340	270	483	316	96	299	362	238	471
La	16.30	17.49	15.46	15.79	8.02	15.08	19.16	15.11	16.36
Ce	37.49	40.47	36.74	35.13	17.13	33.80	40.84	33.79	36.96
Pr	4.71	5.09	4.64	4.41	2.05	4.26	5.27	4.26	4.66
Nd	20.58	21.74	20.30	19.09	9.24	18.18	22.68	18.73	20.28
Sm	4.38	4.67	4.48	4.16	2.37	4.17	5.05	4.04	4.45
Eu	1.22	1.37	1.44	1.21	0.70	1.26	1.45	1.16	1.43
Gd	4.14	4.24	4.28	3.91	2.79	4.07	5.87	3.99	4.31
Tb	0.60	0.57	0.59	0.59	0.47	0.60	0.87	0.58	0.61
Dy	3.67	3.75	3.87	3.46	3.24	3.79	5.57	3.52	3.94
Ho	0.78	0.78	0.81	0.70	0.68	0.77	1.19	0.74	0.83
Er	2.27	2.20	2.41	2.22	2.04	2.28	3.51	2.17	2.39
Tm	0.33	0.32	0.35	0.29	0.29	0.33	0.46	0.34	0.33
Yb	2.12	2.09	2.21	1.95	2.10	2.11	2.86	2.12	2.25
Lu	0.33	0.32	0.32	0.30	0.26	0.30	0.41	0.35	0.36
Y	19.9	19.9	20.3	19.2	18.3	20.4	31.6	19.4	20.4
Th	2	3	2	3	<1	<1	Nd	2	1
V	250	261	290	194	151	224	258	257	308
Cu	61	29	81	51	99	52	87	119	93
Pb	18	9	13	14	60	22	179	9	9
Eu/Eu*	0.287	0.308	0.329	0.300	0.272	0.305	0.266	0.289	0.326
Zr/Y	2.623	2.985	3.253	2.950	3.242	2.705	2.177	3.178	3.088
Ce/Pb	2.078	4.294	2.776	2.507	0.287	1.506	0.228	3.935	4.219

Yb diagrams (Condie 1989), most of the Lattan Mountain magmatic rocks distribute in the field of arc-related setting (Fig. 10a).

LOI loss on ignition; Eu/Eu* = (Eu)N/((Sm)N × (Gd)N)1/2 (after McLennan 1989)

Sr-Nd isotope geochemistry

The whole-rock Rb-Sr isochron diagram for the LM rocks is shown in Fig. 11a and b. All of the plots showed a clear isochron with an age of 152 ± 37 Ma and an initial ratio of

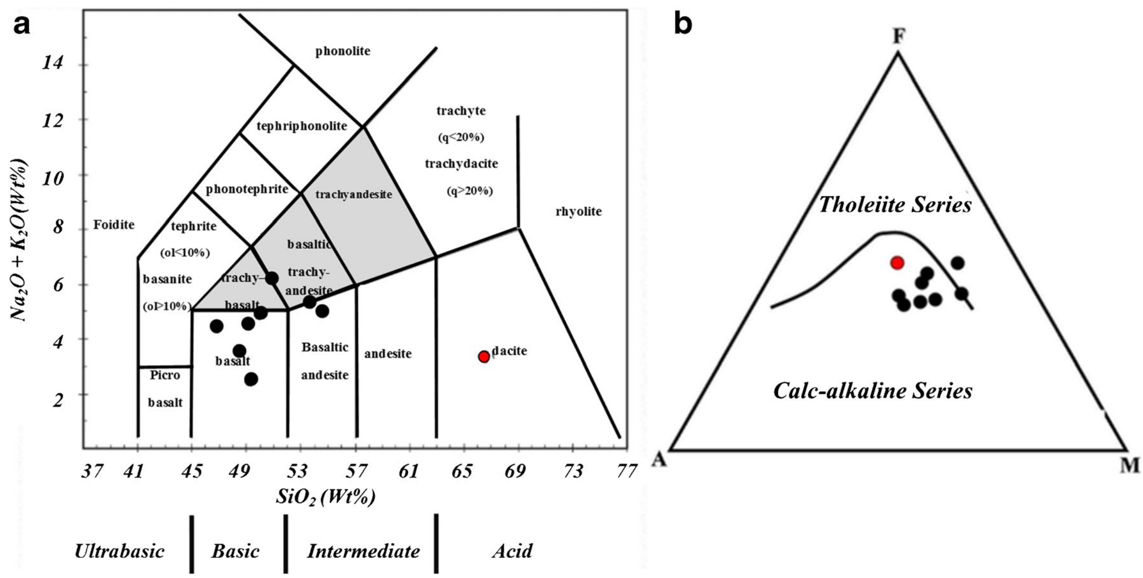

Fig. 5 Chemical classification diagrams for the LM samples: **a** Le Bas (2000). **b** AFM diagram (Irvine and Baragar 1971). Black circle, mafic and intermediate samples; red circle, dacite sample

0.7048 (MSDW = 0.19). Isochron samples without dacite showed an age of 152 ± 14 Ma and an initial ratio of 0.7048 (MSDW = 0.19). Isotopic data of the igneous rocks in the LM area at 152 Ma displayed homogeneous values for the initial isotope ratios: εNdt values were from − 0.08 to + 2.19 and Sr isotope ratios ($^{87}Sr/^{86}Sr$)i were between 0.7047 and 0.7051

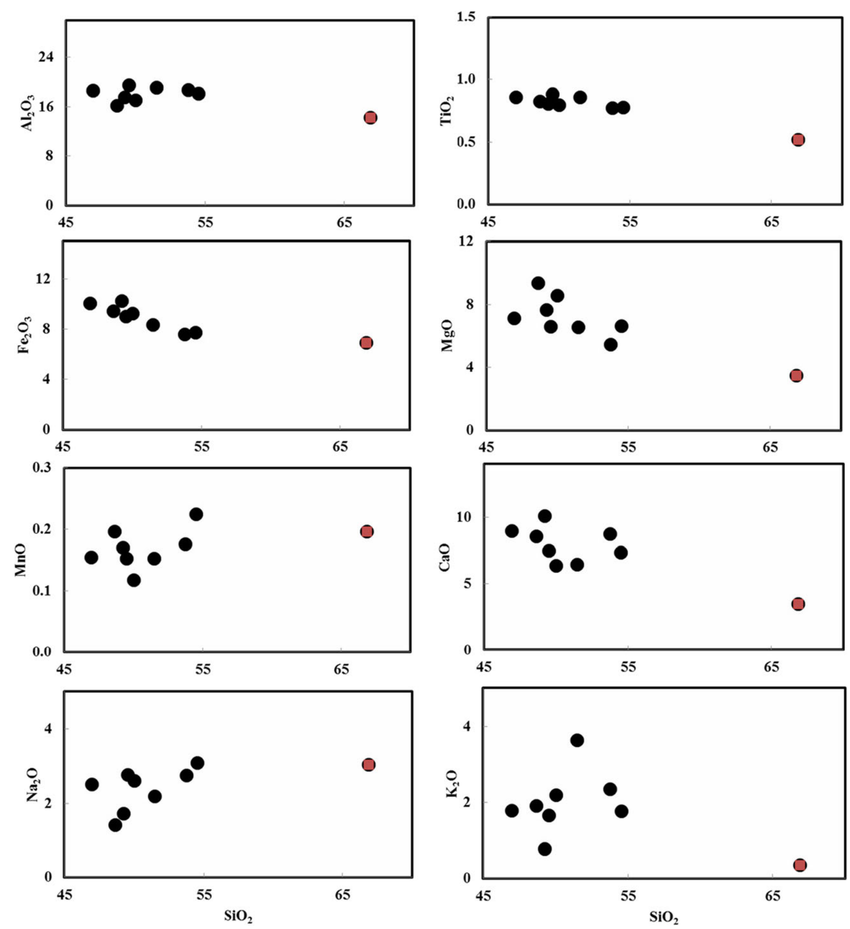

Fig. 6 Harker (1909) diagrams of LM samples. Black circle, mafic and intermediate samples; red circle, dacite sample

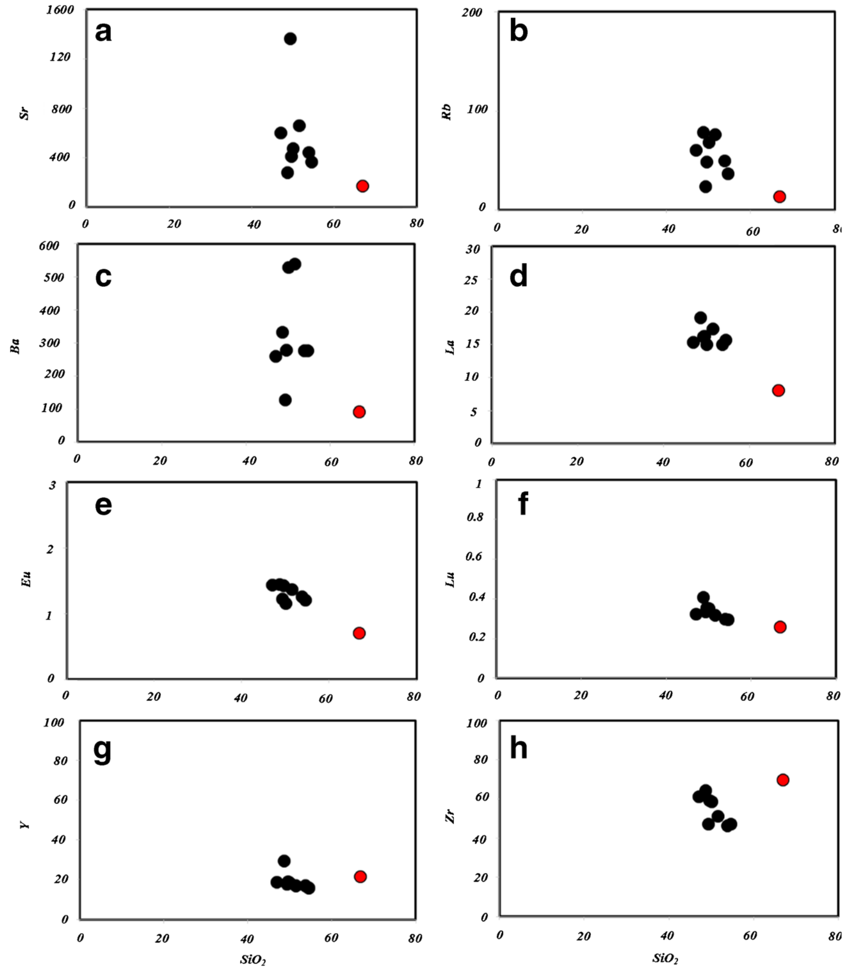

Fig. 7 Harker diagrams of the LM samples (Harker 1909). Black circle, Mafic and intermediate samples; red circle, dacite sample

(Table 2). In the $^{143}Nd/^{144}Nd$–$^{87}Sr/^{86}Sr$ diagram, all of the samples were plotted in the mantle array field extending to the BSE nature (Fig. 12).

The Nd and Sr natural isotope ratios were normalized based on the $^{146}Nd/^{144}Nd$ and $^{86}Sr/^{88}Sr$ = 0.1194. The average and 2σ for isotope ratios standards are NIST-SRM987 = 0.710251

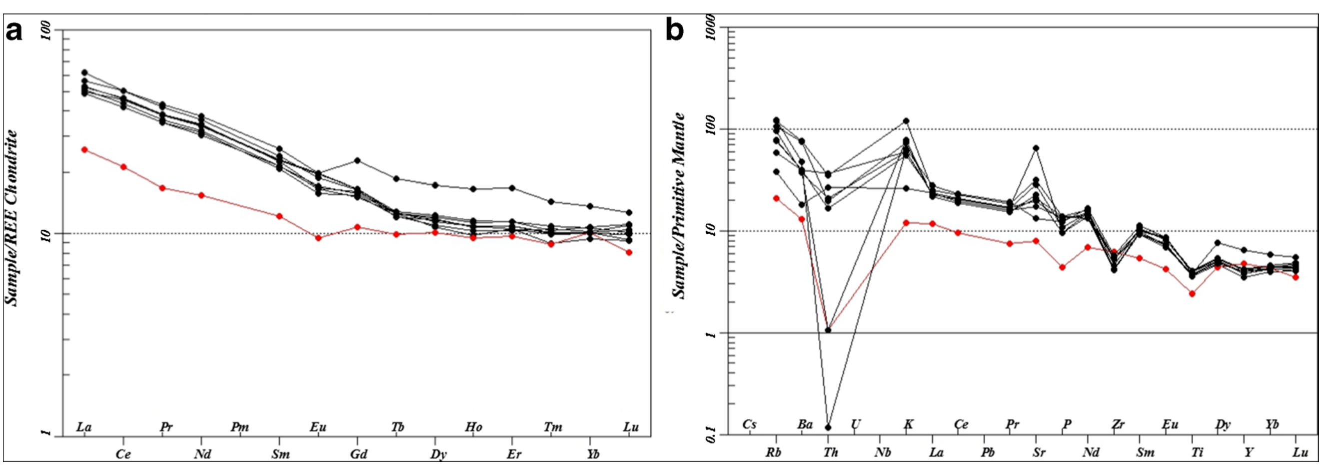

Fig. 8 **a** Chondrite-normalized REE patterns (Boynton 1984). **b** Primitive mantle-normalized extended trace element spider patterns of the LM samples (McDonough and Sun 1995). Black circle, mafic and intermediate samples; red circle, dacite sample

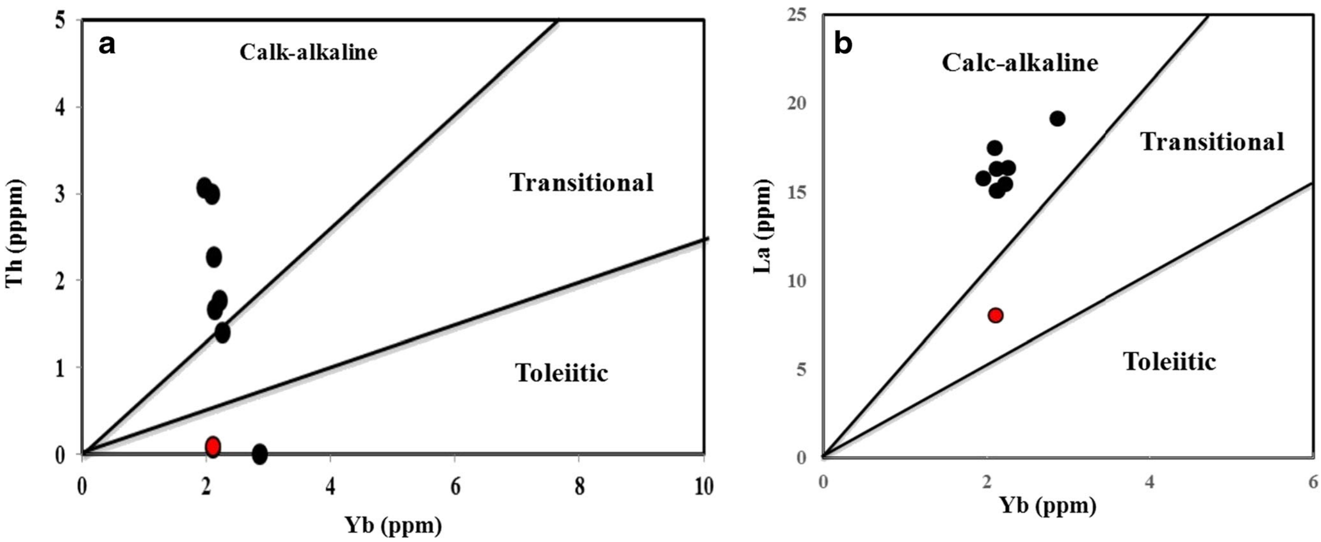

Fig. 9 For the LM samples: **a** Th vs. Yb diagram (Barrett and MacLean 1999); **b** La vs. Yb diagram (Ross and Bédard 2009). Black circle, mafic and intermediate samples; red circle, dacite sample

± 0.000020 ($n = 8$) and JNdi-1 = 0.512114 ± 0.000002 ($n = 6$). The CHUR (chondritic uniform reservoir) values, $^{143}Nd/^{144}Nd$ = 0.51247, were used to calculate the εNd. εNd(t) (DePaolo and Wasserburg 1976) were calculated based on the following: $(^{143}Nd/^{144}Nd)TCHUR = 0.512638–0.1967(e^{\lambda T} - 1)$

Discussion

The LM igneous rocks are basic to intermediate, with a feature of calc-alkaline series. The major element trends for Al_2O_3, Fe_2O_3, TiO_2, CaO, and MgO in the Harker diagrams had a negative correlation, which indicate to chemical evolution of magma by crustal contamination. Also, Sr, Rb, Ba, Y, Zr, Lu, and La behavior ratio to SiO_2 indicates alteration and an incompatibility of the element as the magma differentiation increases (Barclay and Carmichael 2004; Moore and Carmichael 1998; Sisson and Grove 1993). The Sr, Rb, Pb enrichment indicates presence a subducted oceanic plate for the occurrence of the magmatic rocks (Wang et al. 2016). In Zr/Al_2O_3 vs. TiO_2/Al_2O_3 and La/Yb vs. Th/Yb diagrams (Condie 1989), most of the Lattan Mountain magmatic rocks distribute in the field of arc-related setting (Fig. 10a). There are three potential sources for magma production in the arc magmatism increasing LREE relative to HREE, including (1) low partial melting of the mantle wedge source (Almeida et al. 2007), (2) crustal contamination of the magma (Almeida et al. 2007), and (3) released fluid or melt of slab (Winter 2001). The released melt and aqueous fluids from subducted slabs can enrich

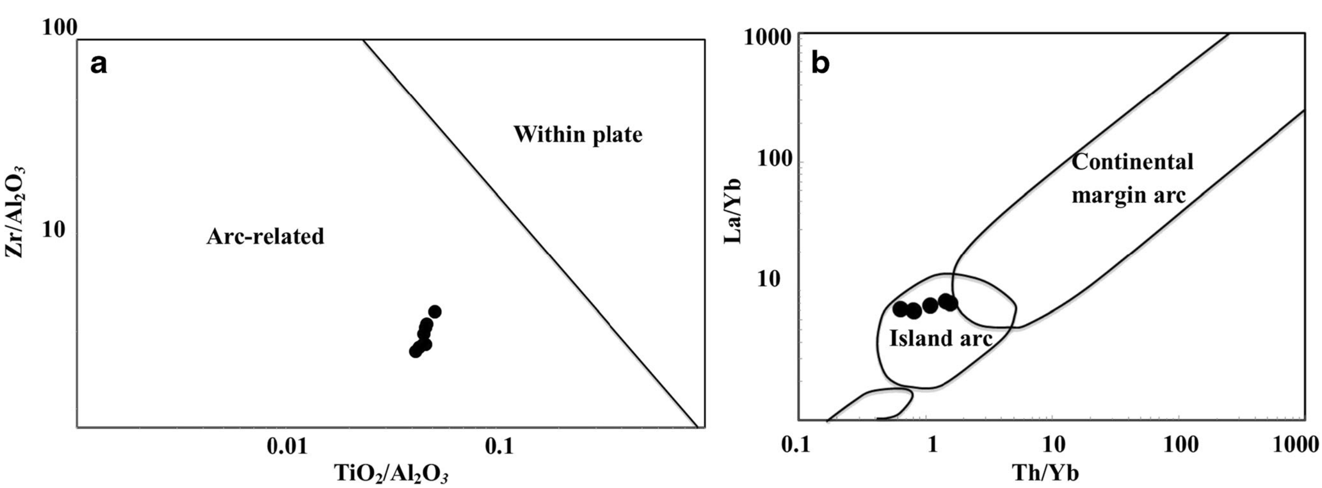

Fig. 10 Tectonic setting discrimination diagrams showing arc-related tectonic setting for these rocks. **a** Zr/Al_2O_3 vs. TiO_2/Al_2O_3. **b** La/Yb vs. Th/Yb (Condie 1989)

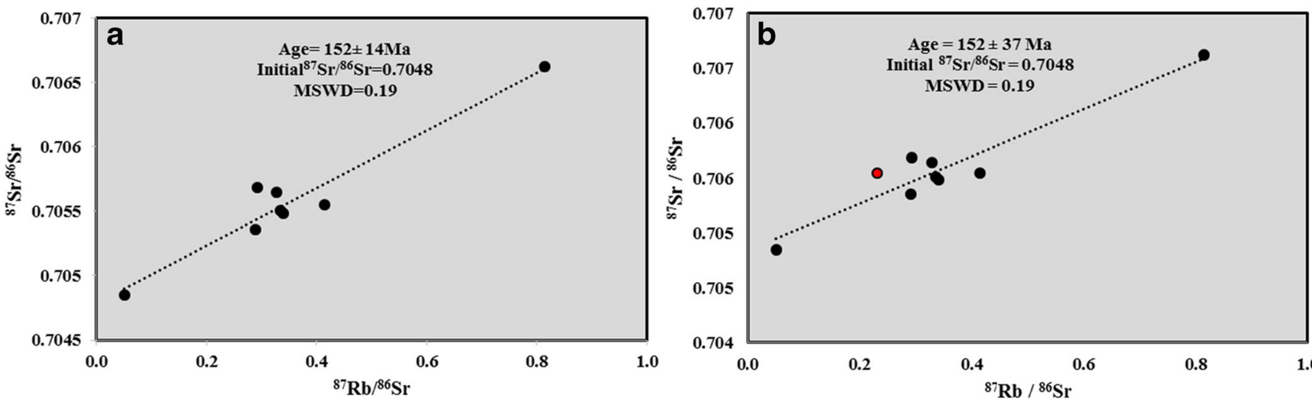

Fig. 11 Whole-rock Rb-Sr isochron diagram for the LM rocks. **a** 8 samples without dacite. **b** All of samples. Black circle, mafic and intermediate samples; red circle, dacite sample

the mantle wedge by metasomatism (Kepezhinskas et al. 1995; McInnes et al. 2001; Pearce and Peate 1995; Rapp et al. 1999). The Th/Yb vs. Th and La/Yb vs. La diagrams show that partial melting is a dominant process in magma generation. It is confirmed by depletion of Ti with respect to other HFS elements that can be explained by derivation from a source with small-degree partial melts. The behavior Th in the diagram (Fig. 7a) shows an increase of the Th with the increase of the sample silica that due to sedimentary of the subducted slab (Gorton and Schandl 2000). In addition, Th behavior is due to high separation coefficient values (0.15) by amphibole in the andesitic melt (Rollinson 1993). Low Sr/Y ratio (8.81–68.54 ppm) indicated to mantel wedge as the major factor in the magmatic source (Munker et al. 2004) and low Zr/Y < 3 indicated to arc island as geology setting (Pearce and Norry 1979). Also, the Nd/Pb (< 10) and Ce/Pb (< 10) indicate presence of the slab-derived fluids (Bonev and Stampfli 2008). The La/Yb > 6 shows calc-alkaline to transitional nature of the LM magmatic rocks (Barrett and MacLean 1999). According to the Sr-Nd data, these rocks are formed by a magma source similar to BSE. All of the data show that LM igneous rocks are formed by subduction zone in 152 Ma years ago. This age is correlated with the magmatism of Jurassic–Cretaceous SaSZ. Arc magmatism is the most distinctive component in the SaSZ and includes voluminous calc-alkaline plutons and volcanic rocks, mainly at Jurassic age around 170 Ma (Hassanzadeh and Wernicke 2016). Azizi and Asahara (2013) attributed the temporal cessation and spatial shift in magmatism to a Jurassic arc-continent collision. These authors suggested that the intra-oceanic forearc is no longer present because it was removed by subsequent tectonic erosion during Cenozoic subduction, continental collision, and strike-slip faulting (Mohajjel and Fergusson 2000). Yajam et al. (2015) suggest that the calc-alkaline I-type to alkaline A-type transition in the SSZ was the result of a change from compressional subduction and arc collision to extensional rifting. As mentioned above, Azizi and Asahara (2013) suggested that an island arc collided with the SaSZ in the Late Jurassic. As a result of any of the suggested processes, the Late Jurassic calc-

Table 2 Sr and Nd isotopic compositions of the LM samples

Sample	$^{87}Rb/^{86}Sr$	$^{87}Sr/^{86}Sr$	$(^{87}Sr/^{86}Sr)i$	$^{147}Nd/^{144}Nd$	$^{143}Nd/^{144}Nd$	$(^{143}Nd/^{144}Nd)t$	εNd(t)
La1	0.051	0.704851	0.704742	0.128544	0.512609	0.512483	0.73947
La2	0.33	0.705508	0.704794	0.129891	0.512598	0.512471	0.49902
La3	0.29	0.705354	0.704735	0.133491	0.512616	0.512485	0.78132
La4	0.29	0.705689	0.705064	0.131625	0.512615	0.512486	0.79756
La5	0.23	0.705542	0.705049	0.155399	0.51271	0.512557	2.19606
La6	0.33	0.705645	0.704946	0.138824	0.512616	0.512480	0.67918
La7	0.81	0.706621	0.704885	0.134698	0.512573	0.512441	– 0.08-092
La8	0.41	0.705548	0.704665	0.130552	0.51263	0.512502	1.11081
La9	0.34	0.705484	0.704759	0.132749	0.512618	0.512488	0.83456

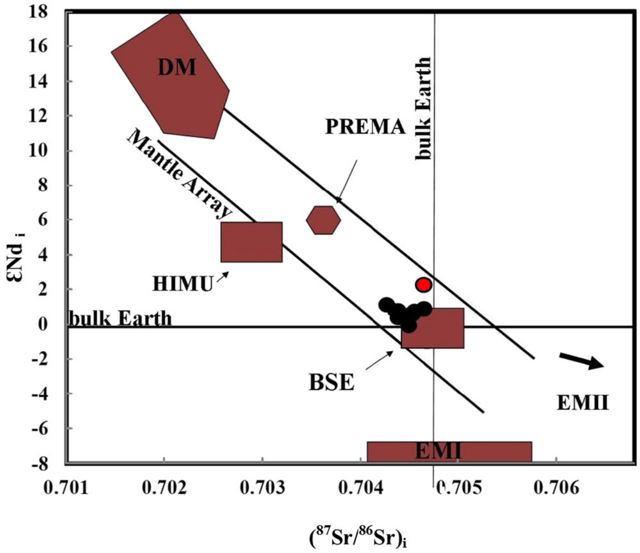

Fig. 12 εNdi vs. $^{87}Sr/^{86}Sr$ diagram for the Lattan Mountain samples (DePaolo and Wasserburg 1976). DM, depleted mantle; PREMA, primary mantle; EMI, enriched mantle (type I); EMII, enriched mantle (type II); HIMU, anomaly high $^{238}U/^{204}Pb$ mantle; BSE, bulk silicate earth; PREMA, prevalent mantle; black circle, mafic and intermediate samples; red circle, dacite sample

alkaline reflects a perturbation of the northeastward subduction of Neotethys beneath the Iranian sector of Eurasia, Laurasia.

Conclusion

Volcanic (basalt, andesite, basaltic andesite, and dacite), subvolcanic (dolerite), and plutonic (microdiorite and microgabbro) rocks in LM show calc-alkaline to transitional affinity. Isotopic composition of samples is similar to mantel array magmas with the affinity to BSE. LM magmatic rocks were formed by subduction process and the closure of the Neotethys ocean plate at around 152 Ma similar to other parts of the SaSZ such as the north of SaSZ in the arc setting. The dominant process for occurrence is partial melting of mantle wedge by released fluid or melt from sedimentary rocks.

Acknowledgments The authors gratefully acknowledge careful and detailed reviews by Dr. Federico Lucci and an anonymous reviewer. We give special thanks to the Head of the Department of Earth and Environmental Sciences, Nagoya University, and the Department of Applied Chemistry for Environment, School of Science and Technology, Kwansei Gakuin University, in Japan for ICP and isotope dating.

References

Alavi A (2004) Regional stratigraphy of the Zagros fold-thrust belt of Iran and its proforeland evolution. Am J Sci 304:1–20

Alavi M (1994) Tectonics of the zagros orogenic belt of iran: new data and interpretations. Tectonophysics 229(3–4):211–238

Almeida ME, Macambira MJB, Oliveira EC (2007) Geochemistry and zircon geochronology of the I-type high-K calc-alkaline and S-type granitoid rocks from southeastern Roraima, Brazil: Orosirian collisional. Precambrian Res 155:69–97

Azizi H, Asahara Y (2013) Juvenile granite in the Sanandaj-Sirjan Zone NW Iran: Late Jurassic-Early Cretaceous arc-continent collision. Int Geol Rev 55:1523–1540

Azizi H, Jahangiri A (2008) Cretaceous subduction-related volcanism in the northern Sanandaj-Sirjan Zone Iran. J Geodyn 45:178–190

Azizi H, Asahara Y, Mehrabi B, Chung SL (2011) Geochronological and geochemical constraints on the petrogenesis of high-K granite from the Suffi Abad area, Sanandaj-Sirjan Zone, NW Iran. Chemie der Erde-Geochemistry 71:363–376

Azizi H, Asahara Y, Tsuboi M, Takemura K, Razani S (2014) The role of heterogenetic mantle in the genesis of adakites northeast of Sanandaj northwestern Iran. Chem Erde 74:87–97

Azizi H, Najari M, Asahara Y, Catlos EJ, Shimizu M, Yamamoto K (2015a) U–Pb zircon ages and geochemistry of Kangareh and Taghiabad mafic bodies in northern Sanandaj–Sirjan Zone, Iran: evidence for intra-oceanic arc and back-arc tectonic regime in Late Jurassic. Tectonophysics 660:47–64

Azizi H, Zanjefili-Beiranvand M, Asahara Y (2015b) Zircon U–Pb ages and petrogenesis of a tonalite–trondhjemite–granodiorite (TTG) complex in the Northern Sanandaj–Sirjan zone, northwest Iran: evidence for Late Jurassic arc–continent collision. Lithos 216–217: 178–195

Azizi H, Mohammadi K, Asahara Y, Tsuboi M, Daneshvar N, Mehrabi B (2016) Strongly peraluminous leucogranite (Ebrahim-Attar granite) as evidence for extensional tectonic regime in the Cretaceous, Sanandaj Sirjan zone, northwest Iran. Chemie der Erde-Geochemistry 76:529–541

Azizi H, Lucci F, Stern RJ, Hasannejad S, Asahara Y (2018a) The Late Jurassic Panjeh submarine volcano in the northern Sanandaj-Sirjan Zone, northwest Iran: mantle plume or active margin? Lithos 308: 364–380

Azizi H, Nouri F, Stern RJ, Azizi M, Lucci F, Asahara Y, Zarinkoub MH, Chung SL (2018b) New evidence for Jurassic continental rifting in the northern Sanandaj Sirjan Zone western Iran: the Ghalaylan seamount southwest Ghorveh. Int Geol Rev. https://doi.org/10.1080/00206814201815359l3

Babaie HA, Ghazi AM, Babaei AA, La Tour TE, Hassanipak AA (2001) Trace element geochemistry of the volcanic rocks of the Neyriz ophiolite Iran. J Asia Earth Sci 19:61–67

Badr A, Davoudian AR, Shabanian N, Azizi H, Asahara Y, Neubauer F, Dong Y, Yamamoto Y (2018) A- and I-type metagranites from the North Shahrekord Metamorphic Complex, Iran: evidence for Early Paleozoic post-collisional magmatism. Lithos 300–301:86–104

Barclay J, Carmichael ISE (2004) A hornblende basalt from western Mexico: water-saturated phase relations constrain a pressure temperature window of eruptibility. J Petrol 45:485–506

Barrett TJ, MacLean WH (1999) Volcanic sequences lithogeochemistry and hydrothermal alteration in some bimodal volcanic-associated massive sulfide systems. Rev Econ Geol 8:101–131

Berberian F, Berberian M (1981) Tectono-plutonic episodes in Iran In: Gupta HK, Delany FM (Eds) Zagros-Hindu Kush-Himalaya: geodynamic evolution. American Geophysical Union Washington DC 5–32

Bonev N, Stampfli G (2008) Petrology geochemistry and geodynamic implications of Jurassic island arc magmatism as revealed by mafic volcanic rocks in the Mesozoic low-grade sequence eastern Rhodope Bulgaria. Lithos 100:210–233

Boynton WV (1984) Cosmochemistry of the rare earth elements: meteorite studies In Rare Earth Element Geochemistry (ed P Henserson) [M]. Elsevier 63–114

Condie KC (1989) Geochemical changes in basalts and andesites across the Archean-Proterozoic boundary: identification and significance. Lithos 23:1–18

Davoudian AR, Genser J, Neubauer F, Shabanian N (2016) $^{40}Ar/^{39}Ar$ mineral ages of eclogites from North Shahrekord in the Sanandaj–Sirjan Zone, Iran: implications for the tectonic evolution of Zagros orogen. Gondwana Res 37:216–240

DePaolo DJ, Wasserburg GJ (1976) Nd isotopic variations and petrogenetic models. Geophys Res Lett 3:249–252

Dercourt J, Zonenshain LP, Ricou LE, Kazmin VG, le Pichon X, Knipper AL, Grandjacquet C, Sbortshikov IM, Geyssant J, Lepvrier C, Pechersky DH, Boulin J, Sibuet JC, Savostin LA, Sorokhtin O, Westphal M, Bazhenov ML, Lauer JP, Biju-Duval B (1986) Geological evolution of the Tethys Belt from the Atlantic to the Pamirs since the Lias. Tectonophysics 123:241–315

Dwijesh R, Rajan S, Ravindra R, Jana A (2011) Microtextural and mineral chemical analyses of andesite–dacite from Barren and Narcondam islands: evidences for magma mixing and petrological implications. J Earth Syst Sci:145–155

Eftekharnejad J (1981) Tectonic division of Iran with respect to sedimentary basins. J Iran Pet Soc 82:19–28

Emami N, Khalili M, Noghreyan M (2009) Determination of tectonomagmatic environment of volcanic and subvolcanic rocks in north of Shahrekord by amphiboles geothermobarometry. Iran Soc Crystallogr Mineral 17:267–278

Esna-Ashari A, Tiepolo M, Valizadeh MV, Hassanzadeh J, Sepahi AA (2012) Geochemistry and zircon U-Pb geochronology of Aligoodarz granitoid complex Sanandaj-Sirjan zone Iran. J Asia Earth Sci 43:11–22

Ghasemi A, Haji Hosseini A, Hosseini M (2005) Geological map of Chadegan. Geol Surv Iran Scale 1:100000

Gorton MP, Schandl ES (2000) From continental to island arc: a geochemical index of tectonic setting for arc—related and within plate felsic to intermediate volcanic rocks. Can Mineral 38:1065–1073

Hafkenschied E, Wortel MJR, Spakman W (2006) Subduction history of the Tethyan region derived from seismic tomography and tectonic reconstruction. J Geophys Res 111

Harker A (1909) The natural history of igneous rocks. Methuen and Co., London

Hassanzadeh J, Wernicke BP (2016) The Neotethyan Sanandaj-Sirjan zone of Iran as an archetype for passive margin-arc transitions. Tectonics 35:586–621

Irvine TN, Baragar WR (1971) A guide to the chemical classification of the common igneous rocks. Can J Earth Sci 8:523–548

Janoušek V, Moyen JF, Martin H, Erban V, Farrow C (2016) Geochemical modelling of igneous processes – principles and recipes in R language. Bringing the power of R to a geochemical community. Springer-Verlag, Berlin

Kazmin VG, Sbortshikov IM, Ricou LE, Zonenshain LP, Boulin J, Knipper AL (1986) Volcanic belts as markers of the Mesozoic-Cenozoic active margin of Eurasia. – In: Aubouin, J., Le Pichon, X. & Monin, A. S., eds.): Evolution of the Tethys. Tectonophysics 123:123–152.

Kepezhinskas PK, Defant MJ, Drummond MS (1995) Na metasomatism in the island-arc mantle by slab melt–peridotite interaction: evidence from mantle xenoliths in the north Kamchatka arc. J Petrol 36:1505–1527

Le Bas MJ (2000) IUGS reclassification of the High-Mg and picritic volcanic rocks. J Petrol 41:1467–1470

Mahmoudi SH, Corfu F, Masoudi F, Mehrabi B, Mohajjel M (2011) U-Pb dating and emplacement history of granitoid plutons in the northern Sanandaj-Sirjan zone, Iran. J Asia Earth 41:238–249

Malek-Mahmoudi F, Davoudian AR, Shabanian N, Azizi H, Asahara Y (2017) Geochemistry of metabasites from the North Shahrekord metamorphic complex, Sanandaj-Sirjan Zone: geodynamic implications for the Pan-African basement in Iran. Precambrian Res 293:56–72

McDonough WF, Sun SS (1995) The composition of the Earth. Chem Geol 120:223–253

McInnes BIA, Gregoire M, Binns RA, Herzig PM, Han-nington MD (2001) Hydrous metasomatism of the New Ireland Arc mantle xenoliths: Part 1. Petrology and geochemistry of fluid-metasomatised peridotites. Earth Planet Sci Lett 188:169–183

McLennan SM (1989) Rare earth elements in sedimentary rocks: influence of the provenance and sedimentary process. Geochem Mineral Rare Earth Elem 21:169–200

Mohajjel M, Fergusson CL (2000) Dextral transpression in late Cretaceous continental collision, Sanandaj-Sirjan zone, western Iran. J Struct Geol 22:1125–1139

Mohajjel M, Fergusson CL, Sahandi MR (2003) Cretaceous–Tertiary convergence and continental collision, Sanandaj–Sirjan zone, western Iran. J Asia Earth Sci 21:397–412

Moore G, Carmichael ISE (1998) The hydrous phase equilibria (to 3 kbar) of an andesite and basaltic andesite from western Mexico: constraints on water content and conditions of phenocrysts growth. Contrib Mineral Petrol 130:304–319

Munker C, Worner G, Yogodzisnki G, Churikova T (2004) Behaviour of high field strength elements in subduction zones: constraints from Kamchatka-Aleutian arc lavas. Earth Planet Sci Lett 224:275–293

Pearce JA, Norry MJ (1979) Petrogenetic implications of Ti, Zr, Y, and Nb variations in volcanic rocks. Contrib Mineral Petrol 69:33–47

Pearce JA, Peate DW (1995) Tectonic implications of the composition of volcanic arc magmas. Annu Rev Earth Planet Sci 23:251–285

Popp RK, Hibbert HA, Lamb WM (2006) Oxy-amphibole equilibria in Ti-bearing calcic amphiboles: experimental investigation and petrologic implications for mantle-derived amphiboles. Am Mineral 91:54–66

Rapp RP, Shimizu N, Norman MD, Applegate GS (1999) Reaction between slab-derived melts and peridotite in the mantle wedge: experimental constraints at 3.8 GPa. Chem Geol 160:335–356

Rollinson HR (1993) Using geochemical data: evaluation, presentation, interpretation. Wiley 325p

Ross PS, Bédard JH (2009) Magmatic affinity of modern and ancient subalkaline volcanic rocks determined from trace-element discriminant diagrams. Can J Earth Sci 46:823–839

Shahbazi H, Siebel W, Pourmoafee M, Ghorbani M, Sepahi AA, Shang CK, Abedini MV (2010) Geochemistry and U–Pb zircon geochronology of the Alvand plutonic complex in Sanandaj–Sirjan Zone (Iran): new evidence for Jurassic magmatism. J Asia Earth 39:668–683

Sisson TW, Grove TL (1993) Experimental investigations of the role of H_2O in calc-alkaline differentiation and subduction zone magmatism. Contrib Mineral Petrol 113:143–166

Tanaka T, Togashi S, Kamioka H, Amakawa H, Kagami H, Hamamoto T, Yuhara M, Orihashi Y, Yoneda S, Shimizu H, Kunimaru T, Takahashi K, Yanagi T, Nakano T, Fujimaki H, Shinjo R, Asahara Y, Tanimizu M, Dragusanu C (2000) JNdi-1: a neodymium isotopic reference in consistency with La Jolla neodymium. Chem Geol 168:279–281

Ustaömer T, Robertson AHF (1999) Geochemical evidence used to test alternative plate tectonic models for pre-Upper Jurassic (Palaeotethyan) units in the Central Pontides, N Turkey. Geol J 34:25–53

Wang C, Dinga L, Zhang LY, Kapp P, Pullen A, Yuea YH (2016) Petrogenesis of Middle–Late Triassic volcanic rocks from the

Gangdese belt, southern Lhasa terrane: implications for early subduction of Neo-Tethyan oceanic lithosphere. Lithos 262:320–333
Whitney DL, Evans BW (2010) Abbreviations for names of rock-forming minerals. Am Mineral 95:185–187
Winter JD (2001) An introduction to igneous and metamorphic petrology. Prentice Hall, New Jersey
Yajam S, Ghalamghash J, Montero P, Scarrow JH, Razavi SMH, Bea F (2015) The spatial and compositional evolution of the Late Jurassic Ghorveh-Dehgolan plutons of the Zagros Orogen, Iran. Geologica Acta 13:25–43
Zahedi M, Rahmati-Ilkhchi M, Vaezipour J (1992) Geological map of the Shahrekord Quadrangle E8. 1:250000, Geological Survey of Iran, Tehran, Iran
Zarasvandi A, Rezaei M, Lentz D, Pourkaseb H, Karevani M (2015) The Kasian volcanic rocks, Khorramabad, Iran: Evidence for a Jurassic Intra-Oceanic island arc in Neo-Tethys ocean. Iran J Sci Technol 39A2:165–178